Journal of Solid State Chemistry **143,** 163–173 (1999)
Article ID jssc.1998.8063, available online at http://www.idealibrary.com on IDEAL®

Magnetic Structure and Spin Reorientation in the Ternary Sulfides, $Ni_xCr_{3-x}S_4$ ($x = \frac{1}{4}, \frac{1}{2}, \frac{3}{4}$)

Anthony V. Powell,*,[1] Douglas C. Colgan,* and Clemens Ritter†

*Department of Chemistry, Heriot-Watt University, Riccarton, Edinburgh EH14 4AS, UK; and †Institut Max von Laue–Paul Langevin, F-38042 Grenoble, France

Received May 19, 1998; in revised form October 13, 1998; accepted October 21, 1998

Powder neutron diffraction data for $Ni_xCr_{3-x}S_4$ ($x = \frac{1}{4}, \frac{1}{2}, \frac{3}{4}$) collected over the temperature range $1.8 \leq T \leq 286$ K demonstrate that all phases exhibit long-range magnetic order at low temperatures. The magnetic ordering temperature is composition dependent and increases with decreasing nickel content (205, 210, and 218 K for $x = \frac{3}{4}, \frac{1}{2}$, and $\frac{1}{4}$, respectively). The magnetic structure determined at 1.8 K involves a doubling of the unit cell in both the *a* and the *c* directions. Moments associated with cations in a fully occupied metal layer, directed parallel to the cation layers, show little compositional dependence, whereas those associated with cations in an ordered vacancy layer are directed toward the anion layers and have a maximum value at the composition corresponding to $x = \frac{1}{2}$. At temperatures between 1.8 K and the ordering temperature, materials with compositions corresponding to $x = \frac{1}{4}$ and $\frac{3}{4}$ show a gradual 90° reorientation of the direction of the vacancy layer moments such that at temperatures just below the ordering temperature, moments lie parallel to the crystallographic *b*-axis. © 1999 Academic Press

INTRODUCTION

The Cr_3S_4 structure (Fig. 1) is an ordered-vacancy structure (1) intermediate between the nickel arsenide and cadmium iodide structure types. Half-occupancy of available octahedral sites between alternate pairs of hexagonally close-packed sulfide layers occurs in an ordered manner, resulting in a two-dimensional superstructure with dimensions related to those of the primitive hexagonal unit cell (a_h) by $\sqrt{3}a_h \times a_h$. The octahedral sites between the remaining pairs of close-packed layers are fully occupied, leading to a stoichiometry of M_3S_4.

This structure is adopted by a variety of stoichiometric ternary transition-metal sulfides of general formula $M'M_2S_4$ (M' = V, Cr, Co, Fe, Ni; M = Cr, Ti, V) (2) for which two extreme cation arrangements, corresponding to the normal $(M)[MM']S_4$ and inverse $(M)[MM']S_4$ structures, can be envisaged: parentheses and square brackets represent sites in the ordered-vacancy and fully occupied layers, respectively. By preparation of nonstoichiometric series $M'_xCr_{3-x}S_4$, we have sought to investigate changes in physical properties which result when Cr(II) in Cr_3S_4 is progressively replaced by an isovalent cation drawn from the first transition series. Substitution with divalent vanadium (3), produces an abrupt change in magnetic and electronic properties at a critical composition corresponding to $x_c \approx 0.4$. This is accompanied by a transition from the near-normal structure, found at low x, to a structure which is intermediate between the normal and inverse types (4). Contrasting behavior is observed when chromium is substituted by divalent nickel, the d^{n+5} analogue of V(II). Preparation of the series $Ni_xCr_{3-x}S_4$ in increments of $x = 0.25$ over the composition range $0 \leq x \leq 1.0$ provided a means of changing the formal electron-count associated with the divalent cation by one for each step in composition (5). Rietveld refinement using room-temperature powder neutron diffraction data demonstrates that, in contrast to the $V_xCr_{3-x}S_4$ series, a near-normal structure is adopted at all compositions: even in the stoichiometric ternary phase, the fully occupied layer contains only ca. 15% of Ni(II). This structural similarity across the series is reflected in the physical properties of these materials. The end-member phase $NiCr_2S_4$ has previously been reported to be a low-activation-energy semiconductor (6). Our data (5) suggest that although $NiCr_2S_4$ is clearly a semiconductor below 300 K, an effectively temperature independent resistivity above this temperature indicates some degree of delocalization of the e_g electrons. Furthermore, all nonstoichiometric phases are, like the other end-member phase Cr_3S_4 (7), metallic. In addition, magnetic susceptibility data (5) suggest that all members of the series possess similar bulk magnetic properties. On cooling from 350 K, the $\chi(T)$ curves exhibit anomalies at temperatures around 200 K before passing through a minimum at ca. 120 K, which is less marked for the $x = 0.25$ phase than for the other phases. In all cases, an

[1] To whom correspondence should be addressed. Fax: +44 (0) 131 451 3180. E-mail: a.v.powell@hw.ac.uk.

0022-4596/99 $30.00

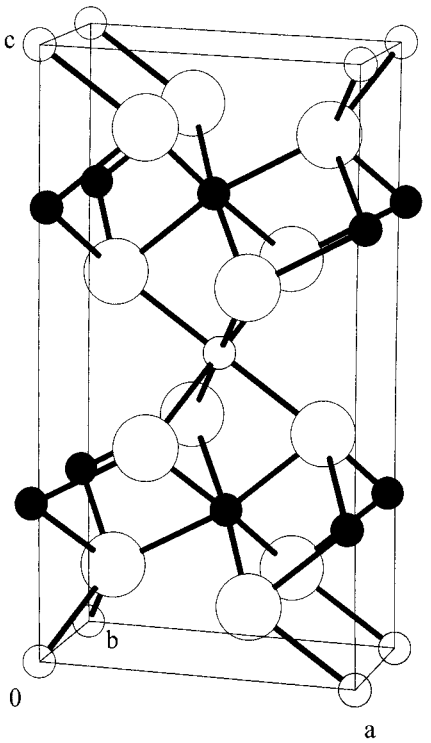

FIG. 1. The Cr_3S_4 structure. Large open circles represent anions, small filled circles represent cations in the fully occupied layer, and small open circles represent cations in the vacancy layer.

increase in measured susceptibility is observed at lower temperatures. A recent variable temperature powder neutron diffraction study on $NiCr_2S_4$ (8) has shown that the broad maximum in susceptibility is associated with the onset of long-range magnetic order at $T = 180$(K). Ordering results in a low-temperature magnetic structure in which the crystallographic unit cell is doubled in the *a*- and *c*-directions. Although differing in the detailed structure, this is similar to that originally proposed by Andron and Bertaut (9). Furthermore, the neutron study indicated that the characteristic shape of the $\chi(T)$ curve below the magnetic ordering temperature could be correlated with the different temperature dependences of the ordered moments associated with the two types of cation site. The similar $\chi(T)$ curves for the nonstoichiometric materials suggests that these phases should exhibit similar magnetic ordering. However, the powder neutron diffraction data presented here illustrate that, contrary to expectation, the thermal evolution of the magnetic structure, at certain compositions, is more complex than that for $NiCr_2S_4$.

EXPERIMENTAL

All samples were prepared by high-temperature reaction at 950°C of appropriate mixtures of the powdered elements in evacuated, sealed silica ampoules. A combination of powder X-ray diffraction, thermogravimetry, atomic absorption spectroscopy, and energy dispersive X-ray microanalysis confirmed all materials to be single phases, with unit cell parameters similar to those previously obtained from single crystal studies (10), and compositions in good agreement with nominal stoichiometries. Full details of the preparation and characterization of these samples have been presented elsewhere (5).

Powder neutron diffraction data were collected over the angular range $20 \leq 2\theta \leq 100^\circ$ with a neutron wavelength of 2.524 Å on the D1B diffractometer at the high-flux reactor, ILL, Grenoble. Approximately 2 g of sample was contained in a thin walled vanadium can, mounted in a standard ILL orange cryostat held at 1.8 K and data collected over a period of 3 h. Variable temperature measurements were made over the range $1.8 \leq T \leq 286$ K by collecting diffraction patterns over 10 min in approximately 10 K temperature increments. Rietveld refinements were carried out using the GSAS package (11) installed on the Heriot-Watt University Alpha 2100–4275 system.

RESULTS

1.8 K Neutron Data

For each composition, the appropriate crystallographic structure previously determined from time-of-flight powder neutron diffraction data collected at 298 K (5) was used for the initial structural model for Rietveld refinement at 1.8 K. Neutron scattering lengths incorporated within GSAS were used. The background was fitted using a cosine Fourier series with the coefficients included as refinable parameters. Diffraction peaks were modeled using a pseudo-Voigt peak shape. Following refinement of a scale-factor, background terms, zero-point, and lattice parameters, two regions of the profile at ca. $2\theta = 40^\circ$ and 72° were excluded from the refinement owing to the presence of weak features which have previously been identified (8) as arising from a trace of Cr_2O_3 impurity and instrumental vanadium

A number of additional reflections were apparent in each of the diffraction patterns. In all cases, these indicated a doubling of the crystallographic unit-cell in both the *a* and the *c* directions consistent with a propagation vector of $(\frac{1}{2}, 0, \frac{1}{2})$ as observed for $NiCr_2S_4$. For each composition, the trial magnetic structure was described in space group $P1$ with parameters derived from the magnetic structure of $NiCr_2S_4$. The angular dependence of the magnetic scattering was described using the free-ion form factors (12) for Ni^{2+}, Cr^{2+}, and Cr^{3+}. The average scattering from each of the two crytallographically independent sites was approximated by the form factor of the majority cation at the particular site, although refinement appeared to be relatively insensitive to the choice of form factor to describe the

scattering from a particular site. Initially all magnetic vector components at each of the two sites were set to nonzero values. Positional parameters refined smoothly, although refinement of thermal parameters resulted in physically unrealistic values with errors comparable to the magnitude of the parameters. This problem appears to be instrumental in origin and is related to the limited Q-range of the data. Manual adjustment of thermal parameters resulted in no significant change in the quality of the refinement or in the values of the other refinable parameters. Thermal parameters were subsequently fixed at their arbitrarily refined values. All three magnetic vector components at each of the two cation sites were introduced into the refinement and allowed to vary independently. In all cases, the y component associated with cations in the vacancy layer and the z component associated with cations in the fully occupied layer refined to values close to zero, the value at which they were subsequently fixed. Peak-shape parameters were introduced into the final cycles of refinement which involved 21 variables and resulted in low weighted residuals. Final observed, calculated, and difference profiles are given in Fig. 2 and Table 1 lists the corresponding refined parameters. The magnetic structure of $Ni_{0.75}Cr_{2.25}S_4$ at 1.8 K is shown in Fig. 3a. The structures of $Ni_{0.5}Cr_{2.5}S_4$ and $Ni_{0.25}Cr_{2.75}S_4$ at this temperature are similar, differing only in the magnitude of the ordered moments at each of the two crystallographic sites.

Variable Temperature Neutron Diffraction Data

Powder neutron diffraction data in the angular range $20 \leq 2\theta \leq 50^\circ$, collected at temperatures between 1.8 and 296 K, are plotted in Fig. 4, in which the evolution of the magnetic peaks with temperature may be observed. The magnetic ordering temperature, T_N, for each phase was established by plotting the intensity of the strong $(\frac{1}{2}, 0, \frac{3}{2})$ magnetic reflection as a function of temperature. Sequential Rietveld refinement was performed on patterns over the entire temperature range studied. Initially those constraints on magnetic vector components determined for the low temperature structure were applied ($\mu_y(M) = 0$, $\mu_z[M] = 0$). Although sequential refinement proceeded smoothly for the composition $Ni_{0.5}Cr_{2.5}S_4$, problems were encountered with the phases corresponding to $x = \frac{1}{4}$ and $x = \frac{3}{4}$. In particular, intensity in the region of $2\theta = 42^\circ$, in which the magnetic $(\frac{3}{2}, 0, -\frac{3}{2})$ reflection occurs, is not well fitted at intermediate temperatures. In both cases, as the temperature is raised, the intensity of this reflection initially increases from its very low value at 1.8 K (Fig. 5), reaches a maximum (105 K at $x = \frac{1}{4}$; 100 K at $x = \frac{3}{4}$) before decreasing smoothly to zero at higher temperatures. This behavior differs from that of the analogous reflection in the profiles of the $x = 1$ and $x = \frac{1}{2}$ phases. For the former, this reflection has no observable intensity at any temperature and for the latter, only a very low intensity below T_N, which does not alter markedly on further cooling. By contrast, in all profiles the intensity of the $(\frac{1}{2}, 0, \frac{3}{2})$ reflection decreases smoothly to zero with increasing temperature.

In an effort to improve the fit between observed and calculated intensities in this region of the profile at intermediate temperatures, the constraints on the magnetic vector components were relaxed such that all three components associated with each of the two cations were allowed to vary freely. Moments associated with sites in the fully occupied layer remain in an orientation parallel with the layer. However, for the moments associated with the cations in the vacancy layer, as the temperature is raised there is a growth in the y-component from its initial value of zero: this is accompanied by a decrease in both the x and the z components such that, in addition to a decrease in the magnitude of the moment with increasing temperature, its orientation changes. Above 105 K ($x = \frac{1}{4}$) or 100 K ($x = \frac{3}{4}$) it has a y-component only. Between these temperatures and the ordering temperatures, only the magnitude of the moment decreases. This behaviour is summarized in Fig. 6 for the $x = \frac{3}{4}$ phase, that of the $x = \frac{1}{4}$ phase being similar. The magnetic structure of $Ni_{0.75}Cr_{2.25}S_4$ at 130 K is compared with that at 1.8 K in Fig. 3.

TABLE 1
Refined Parameters for $Ni_xCr_{3-x}S_4$ phases at 1.8 K

		x in $Ni_xCr_{3-x}S_4$		
		0.25	0.50	0.75
	a (Å)	5.8693(7)	5.891(1)	5.8600(5)
	b (Å)	3.41244(6)	3.41377(9)	3.41243(4)
	c (Å)	11.055(2)	11.101(3)	11.055(1)
	β (°)	91.544(9)	91.67(1)	91.569(6)
(M)	Ni:Cr	0.241:0.759	0.476:0.524	0.713:0.287
	μ_x	0.97(5)	2.6(2)	1.14(5)
	μ_y	0.0	0.0	0.0
	μ_z	− 0.57(6)	− 1.19(9)	− 0.92(7)
	Moment/μ_B	1.12(6)	2.8(2)	1.46(6)
[M]	Ni:Cr	0.004:0.996	0.012:0.988	0.019:0.981
	x	− 0.025(1)	− 0.035(2)	− 0.0265(9)
	z	0.2568(8)	0.2567(9)	0.2595(5)
	μ_x	− 1.96(6)	− 1.8(1)	− 1.90(5)
	μ_y	− 0.5(1)	− 0.5(1)	− 0.85(6)
	μ_z	0.0	0.0	0.0
	Moment/μ_B	2.03(6)	1.9(1)	2.08(4)
S(1)	x	0.338(2)	0.334(3)	0.340(2)
	z	0.367(1)	0.363(1)	0.3652(8)
S(2)	x	0.328(2)	0.348(3)	0.332(2)
	z	0.884(1)	0.884(1)	0.8819(8)
R_{wp}/%		2.6	2.5	1.9

Note. Space group: $I2/m$, (M) on 2(a) (0,0,0), [M] on 4(i) (x,0,z), S(1) and S(2) on 4(i) (x,0,z).

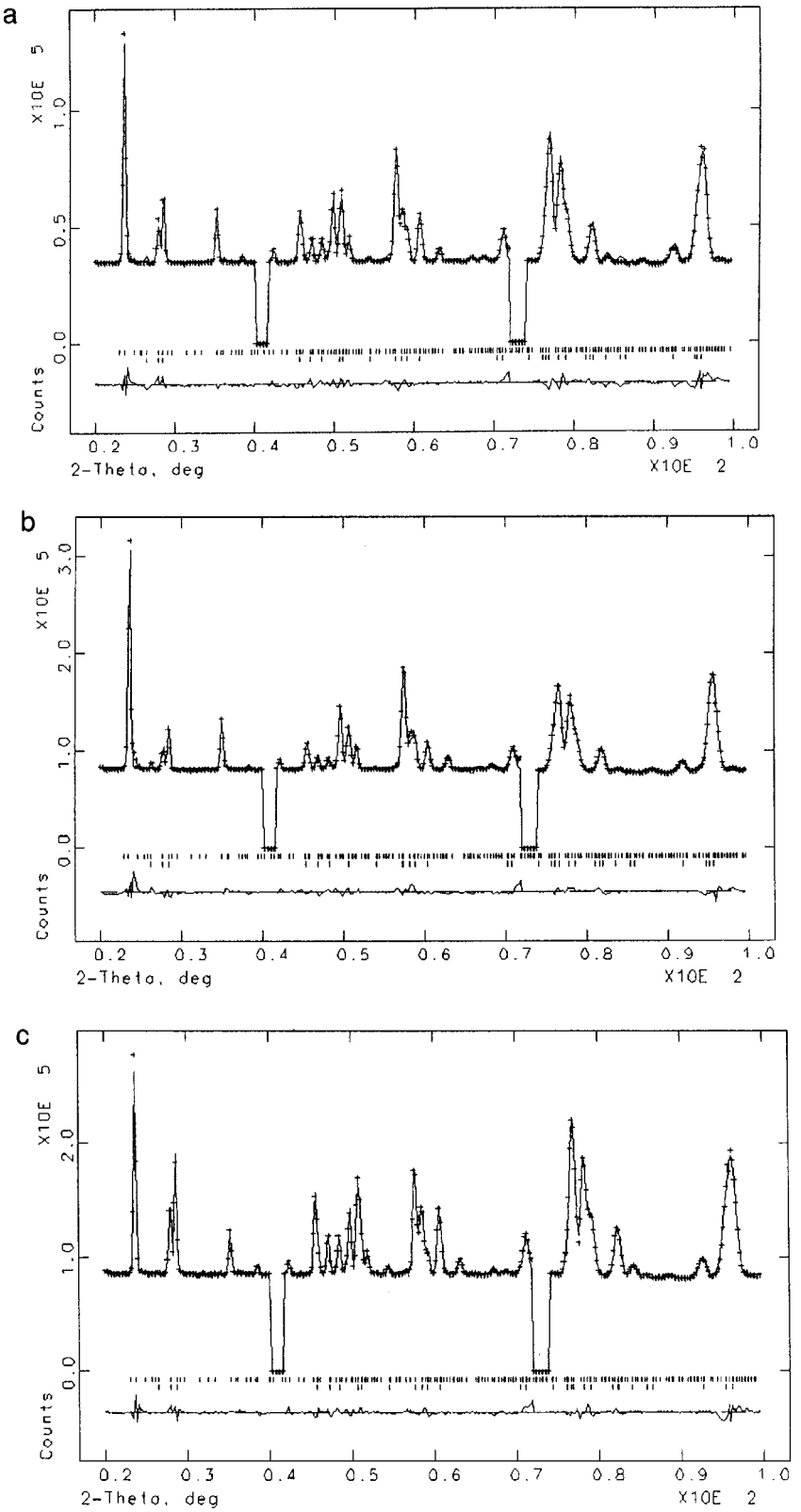

FIG. 2. Final observed (crosses), calculated (full line), and difference (lower full line) neutron profiles for (a) $Ni_{0.25}Cr_{2.75}S_4$, (b) $Ni_{0.5}Cr_{2.5}S_4$, and (c) $Ni_{0.75}Cr_{2.25}S_4$ at 1.8 K. Reflection positions are marked: the lower markers refer to the crystallographic unit cell and the upper markers the magnetic unit cell described in the primitive space group $P1$.

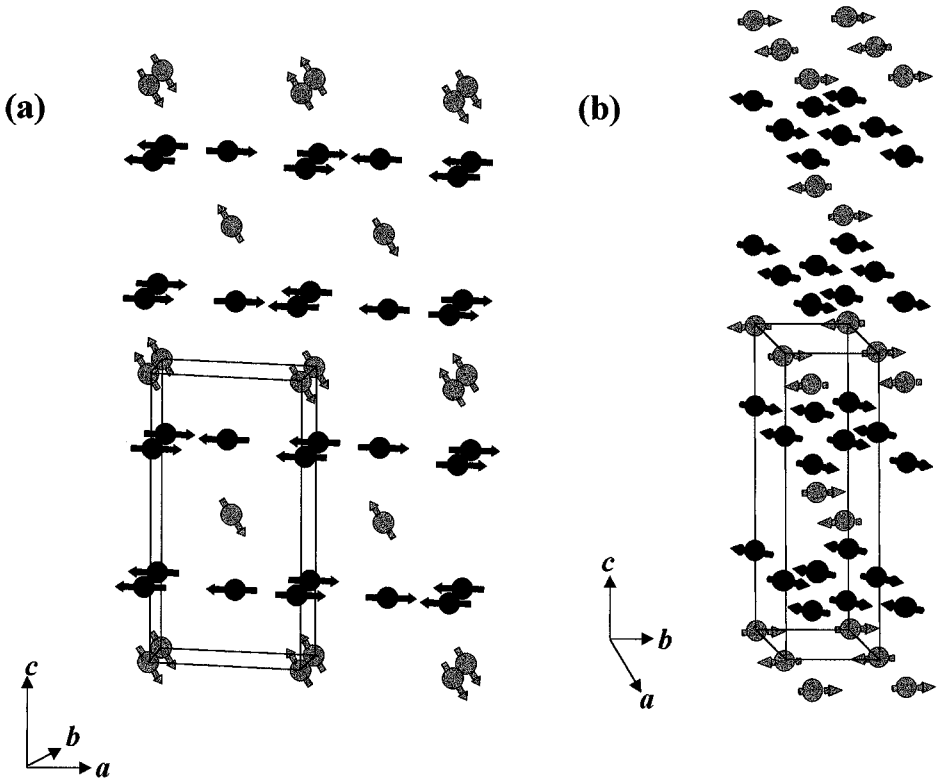

FIG. 3. The magnetic structure of $Ni_{0.75}Cr_{2.25}S_4$ at (a) 1.8 K and (b) 131 K. Cations in the vacancy and fully occupied layer are represented by light and heavy circles, respectively. Sulfide anions are omitted for clarity and the crystallographic unit cell is outlined.

DISCUSSION

The behavior of the unit cell parameters as a function of temperature (Fig. 7) is broadly similar to that previously reported for $NiCr_2S_4$ (8). In particular, whereas the *b*-parameter is effectively constant with temperature, both *a* and *c* decrease with decreasing temperature before appearing to reach a limiting value at ca. 100 K. On cooling from room temperature, the monoclinic distortion initially increases until at temperatures below 100 K, β reaches an approximately constant value. All three phases exhibit a similar temperature dependence of the magnetic moment of the cation in the fully occupied layer. Below the ordering temperature, T_N, the moment initially shows a rapid increase with decreasing temperature, before reaching an apparently limiting value below ca. 100 K (Fig. 8). By contrast, the moment in the vacancy layer shows a less rapid increase with decreasing temperature and in the $x = \frac{1}{2}$ and $x = \frac{3}{4}$ phases continues to increase down to the lowest temperatures studied. Similar behavior of the moments at the two sites as a function of temperature observed in $NiCr_2S_4$ (8) has been used to account for the characteristic form of the magnetic susceptibility curve. The flatter $\mu(T)$ curve for the vacancy layer moment for the $x = \frac{1}{4}$ phase may explain the less pronounced minimum in the plot of magnetic susceptibility *vs* temperature for this material.

Powder neutron diffraction shows that on traversing the series $Ni_xCr_{3-x}S_4$ $0 \leq x \leq 1$, nickel ions replace chromium ions almost exclusively at sites in the ordered vacancy layer. Consequently, if an ionic picture were applicable to these materials, it would be expected that as $Cr^{2+}(S = 2)$ is replaced by $Ni^{2+}(S = 1)$, the average moment associated with cations in the ordered vacancy layer should decrease by 0.5 for each step of $x = \frac{1}{4}$ in composition. Since the fully occupied layer consists almost entirely of $Cr^{3+}(S = \frac{3}{2})$ at all compositions, the moment of cations in this layer would be predicted to show little variation with changing composition. In all three materials investigated here, at 1.8 K the cation in the fully occupied layer possesses a moment of ca. $2\mu_B$. Although this moment is reduced from the spin-only value of $3\mu_B$ expected for an $S = \frac{3}{2}$ ion, the reduction is comparable with that observed by other workers (9, 13) and has been attributed to the appreciable covalency of the Cr–S interaction which results in the transfer of spin density away from the cation. Using the formalism of Hubbard and Marshall (14) an estimate of 8–9% for the covalency parameter is obtained. This is consistent with values obtained for binary chalcogenides (15, 16). A slight further reduction in

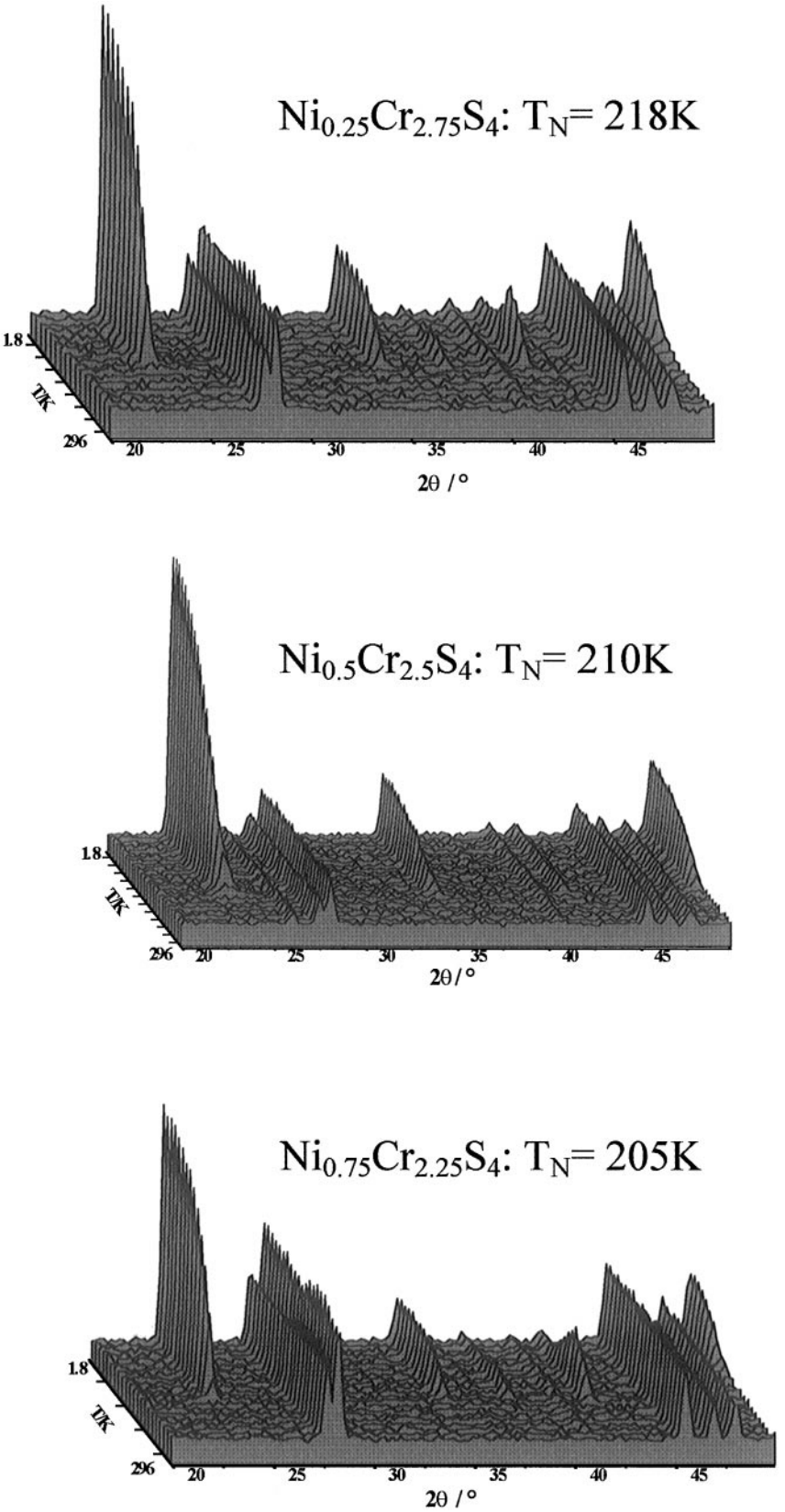

FIG. 4. Powder neutron diffraction data for $Ni_xCr_{3-x}S_4$ over the temperature range $1.8 \leq T \leq 286$ K. Magnetic ordering temperatures, T_N, are indicated.

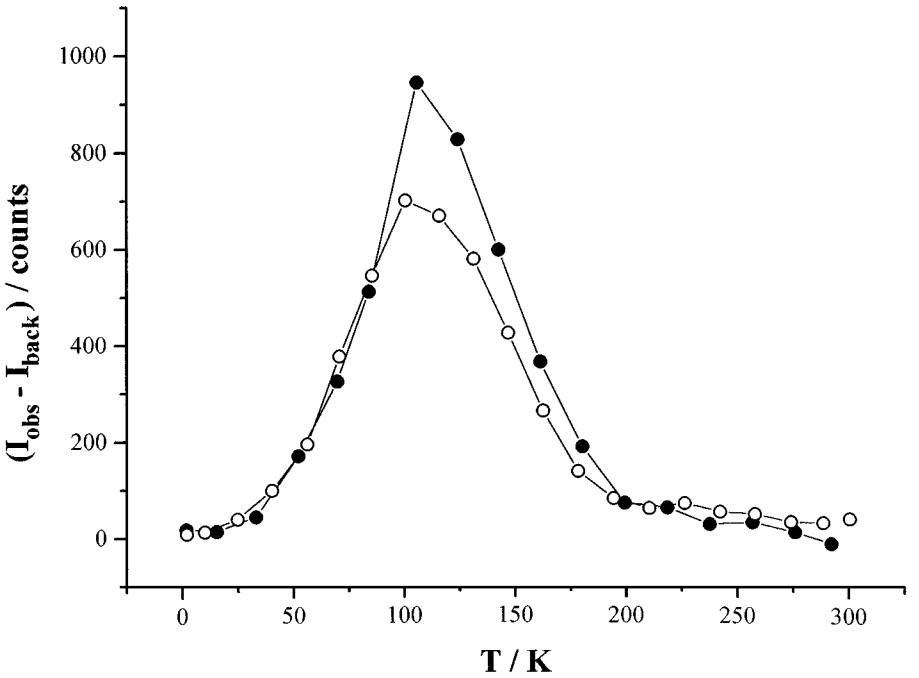

FIG. 5. Temperature dependence of the intensity of the $(\frac{3}{2}, 0, -\frac{3}{2})$ magnetic reflection for $Ni_{0.25}Cr_{2.75}S_4$ (solid points) and $Ni_{0.75}Cr_{2.25}S_4$ (open points). Indices refer to the crystallographic unit cell.

the moment at this site in the end-member phase $NiCr_2S_4$ may be attributed to the larger proportion of nickel ($S = 1$) in the fully occupied layer (ca. 15%) in this material.

The ordered moment of the cations in the vacancy layer exhibits less systematic behavior. Instead of the stepwise decrease, with increasing x, expected on ionic grounds,

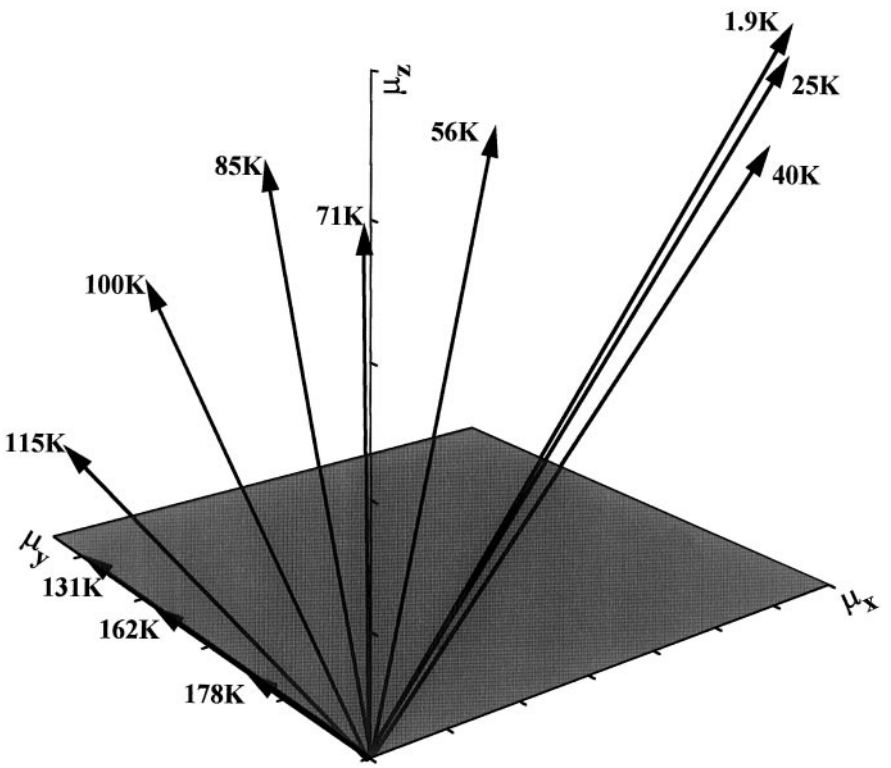

FIG. 6. Reorientation of the magnetic moment, associated with the cation in the vacancy layer in $Ni_{0.75}Cr_{2.25}S_4$, between T_N and 1.8 K.

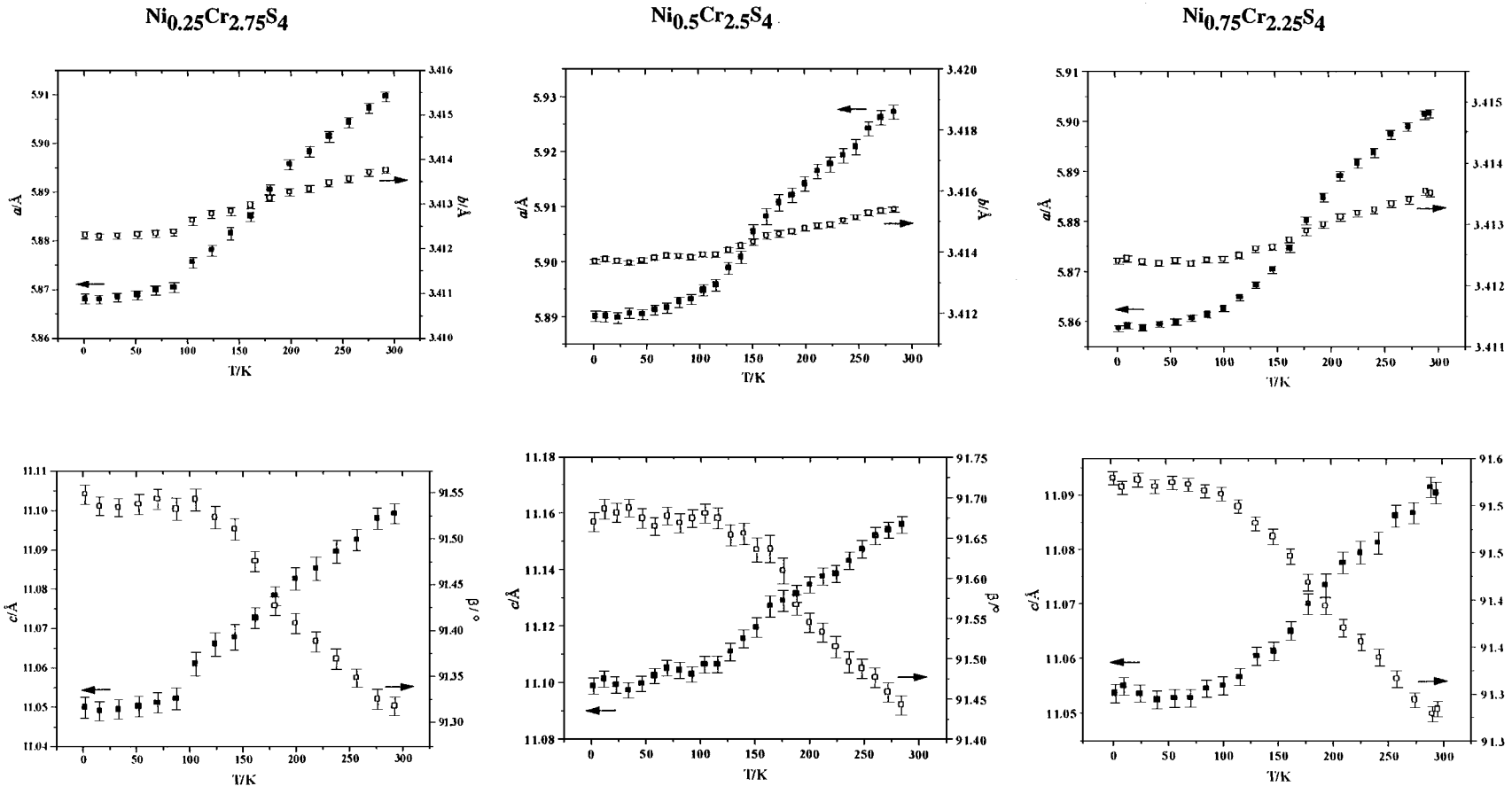

FIG. 7. The temperature dependence of the monoclinic unit-cell parameters of $Ni_xCr_{3-x}S_4$ phases.

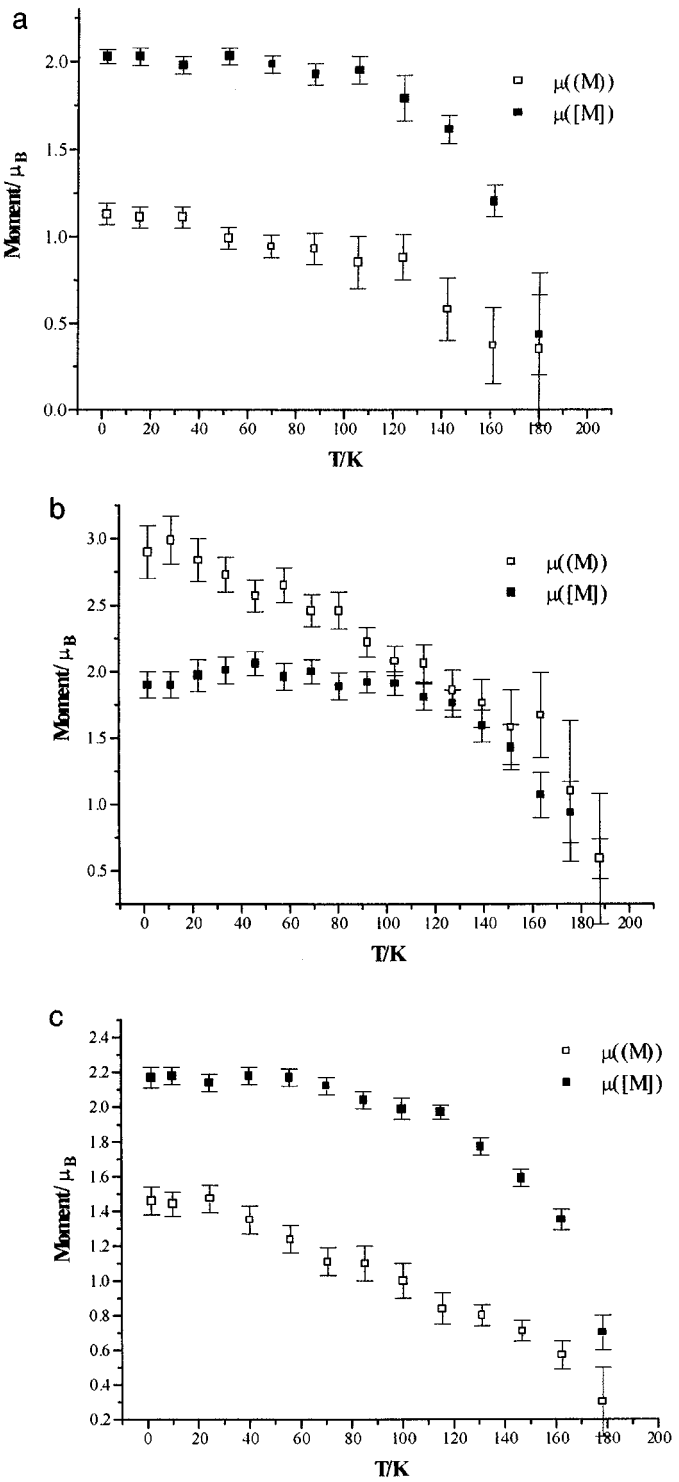

FIG. 8. The temperature dependence of the ordered moments associated with cations at sites in the vacancy (open points) and fully occupied (solid points) layers in (a) $Ni_{0.25}Cr_{2.75}S_4$, (b) $Ni_{0.5}Cr_{2.5}S_4$, and (c) $Ni_{0.75}Cr_{2.25}S_4$.

a maximum value of $2.8\mu_B$ is reached at 50% substitution. At all compositions, the vacancy layer moment is significantly reduced from the weighted average of the spin-only values for Ni^{2+} and Cr^{2+} ions. In the case of $Ni_{0.25}Cr_{2.75}S_4$ this reduction results in a moment which is only ca. 30% of the predicted value. Andresen (17) has reported similarly low values of 1.08 and $0.71\mu_B$ for the ordered moments of cations in the fully occupied and ordered vacancy layers, respectively, in the isostructural selenide, Fe_3Se_4. Such behavior has also been observed in structurally related ordered defect binary chalcogenides (18, 19), including the extreme case of a moment of $0.14\mu_B$ for the vacancy layer cation in Cr_2Te_3 (20). These observations suggest that an ionic description is not wholly applicable to these materials and that electrons reside in narrow bands. This would result in significant electron delocalization which is consistent with the observed metallic behavior (5) of the materials investigated here. The magnetic properties of electrons in narrow band systems depend on factors such as bandwidth, position, and filling (21, 22). Although quantitative analysis of the moments in such systems require detailed band structure calculations to be performed, some qualitative conclusions may be drawn. Narrow bands may result from admixture of anion orbitals with cation *d*-orbitals of the correct symmetry or, at sufficiently short cation–cation separations, by overlap of cation *d*-orbitals. Crystal field effects remove the degeneracy of the octahedral cation *d*-levels, while intraatomic exchange removes the spin degeneracy of the resulting t_{2g} and e_g levels. In a one-electron energy level diagram, this results in the formation of α and β sub-bands for each of the t_{2g} and e_g levels (7). However, band structure calculations, performed for the isostructural materials Cr_3X_4 (X = Se, Te) (23, 24), reveal that significant t_{2g}–t_{2g} orbital interactions occur between cations in the vacancy and fully occupied layers which lie at the centers of octahedra which share a common face. Consequently, one component of the t_{2g} subband shows significant dispersion along the crystallographic *c*-direction. If the resultant broadening is sufficient for the bottom of the $t_{2g}(\beta)$ subband to lie below the Fermi level, E_F, partial cancellation of the majority (α) spin will occur. This may be the cause of the very low moment observed for the vacancy layer cation in $Ni_{0.25}Cr_{2.75}S_4$. Further replacement of Cr(II) with Ni(II) alters the position of E_F, and the resultant moment will depend on the different number of occupied majority (α) and minority (β) spin states. The increased vacancy layer moment in $Ni_{0.5}Cr_{2.5}S_4$ suggests that at this degree of band-filling, there is a high density of states associated with the cation α-levels at E_F, whereas in $Ni_{0.75}Cr_{2.25}S_4$ this is offset by an increase in the number of occupied β-states. In addition to changes in band filling, progressive replacement of Cr(II) with Ni(II) is likely to reduce orbital overlap in the *c*-direction, owing to the effects of orbital contraction. The concomitant band narrowing may account for the semiconducting behavior of $NiCr_2S_4$ and a vacancy layer moment of $1.4\mu_B$, which more closely approaches the value expected for a localized electron description.

The long-range magnetic structure determined at 1.8 K for these materials (Fig. 3a) is similar to that previously determined for $NiCr_2S_4$ (8) and may be described in terms of sheets of cations parallel to the $(10\bar{1})$ planes in which moments are ferromagnetically aligned. Adjacent sheets are coupled antiferromagnetically with respect to each other. This structure differs slightly from that originally proposed by Andron and Bertaut (9) in which all moments, irrespective of cation site, lie in the *ab* plane directed at 45° to the $[10\bar{1}]$ direction such that the projection of the moment on the $(10\bar{1})$ plane made an angle of 122° with the crystallographic *b* axis. Although in the structure described here, moments associated with cations in the fully occupied layer ($\mu[M]$) are in a similar orientation, moments associated with sites in the ordered vacancy layer ($\mu(M)$) lie in the *ac* plane directed at an angle of 114–127° (depending on composition) to the [001] direction. This is a similar orientation to that proposed for both the Cr(II) and Cr(III) moments in the low temperature magnetic structure of Cr_3S_4 (25). The important feature of this structure appears to be the presence in the fully occupied layer of both ferromagnetic and antiferromagnetic exchange interactions. Although the magnitudes of the moments indicate that a narrow band picture is more applicable than a model based on localized electrons, the sign of individual magnetic exchange interactions may be predicted using the same qualitative coupling rules (26). In the nonstoichiometric materials, less than 2% of nickel resides in this layer; these interactions are therefore almost entirely those between Cr(III). Ferromagnetic exchange, arising from a 90° cation–anion–cation superexchange dominates at longer cation–cation distance, whereas antiferromagnetic exchange, due to direct cation–cation interactions, is more significant at shorter separations. Each Cr(III) in the fully occupied layer has six nearest neighbor Cr(III) ions: two each at ca. 3.1, 3.4, and 3.7 Å. Cations separated by the shortest of these distances exhibit antiferromagnetic coupling, whereas at the two longer separations, ferromagnetic exchange occurs.

The $x = \frac{1}{4}$ and $x = \frac{3}{4}$ phases exhibit a spin reorientation, not observed in the $x = \frac{1}{2}$ and $x = 1$ materials, between the ordering temperature and 1.8 K. This involves a 90° rotation of the vacancy layer moment from an initial direction parallel to the crystallographic *b* axis (Fig. 3b) to the *ac* plane (Fig. 3a). Competition between different anisotropic terms, including single-ion effects, dipolar and pseudo-dipolar interactions, has been shown to be responsible for spin reorientation transitions observed in a number of oxide and intermetallic systems (27–29). The vacancy layer cation in $Ni_xCr_{3-x}S_4$ has two cation neighbours in the fully occupied layer at a distance of ca. 2.8 Å and two in the same layer at ca. 3.41 Å. This anisotropic environment will give rise to an exchange field in which components parallel and perpendicular to the vacancy layer are likely to differ considerably. The latter is unlikely to vary greatly with composition owing to the effectively constant composition of the fully occupied layer. This component appears to dominate at low temperature in all cases, with the result that the vacancy layer moments are directed toward the fully occupied layers. However, if this component decreases more rapidly with increasing temperature than the in-plane component, the latter can dominate above a certain temperature and a spin reorientation transition will occur. As the composition of the vacancy layer is dependent on *x*, it might be expected that the in-plane component will vary as the series is traversed. The only apparent structural difference between the three materials studied is in the coordination geometry of the vacancy layer cation. In the $x = \frac{1}{2}$ phase, metal–sulfur distances are slightly greater and the MS_6 octahedron is more regular than in the $x = \frac{1}{4}$ and $x = \frac{3}{4}$ materials. This would lead to differences in the crystalline electric field experienced by the vacancy layer cation at 50% substitution. It appears that at $x = \frac{1}{4}$ and $x = \frac{3}{4}$, the fall-off with increasing temperature of the in-plane component of the exchange field is sufficiently slow to favor an arrangement in which the spins lie parallel to the vacancy layer.

ACKNOWLEDGMENTS

Financial support from the EPSRC is gratefully acknowledged. D.C.C. thanks Heriot–Watt University for a studentship.

REFERENCES

1. F. Hulliger, *Struct. Bonding* **4,** 83 (1968).
2. A. Wold and K. Dwight *in* "Solid State Chemistry: Synthesis, Structure and Properties of Selected Oxides and Sulfides," Chap. 11. Chapman and Hall, New York, 1993.
3. A. V. Powell and S. Oestreich, *J. Mater. Chem.* **6,** 807 (1996).
4. D. C. Colgan and A. V. Powell, *J. Mater. Chem.* **6,** 1579 (1996).
5. D. C. Colgan and A. V. Powell, *J. Mater. Chem.* **7,** 2433 (1997).
6. R. J. Bouchard and A. Wold, *J. Phys. Chem. Solids* **27,** 591 (1966).
7. S. L. Holt, R. J. Bouchard, and A. Wold, *J. Phys. Chem. Solids* **27,** 755 (1966).
8. A. V. Powell, D. C. Colgan, and C. Ritter, *J. Solid State Chem.* **134,** 110 (1997).
9. B. Andron and E. F. Bertaut, *J. Phys.* (*Paris*) **27,** 619 (1966).
10. H. D. Lutz and K. H. Bertram, *Z. Anorg. Allg. Chem.* **401,** 185 (1973).
11. A. C. Larson and R. B. von Dreele, "General Structure Analysis System," Los Alamos Laboratory Report, LAUR 86-748. 1994.
12. P. J. Brown, *in* "International Tables for Crystallography" (A. J. C. Wilson, Ed.), Vol. C, Chap. 4. Kluwer, Dordrecht, 1992.
13. B. Andron and E. F. Bertaut, *J. Phys.* (*Paris*) **27,** 626 (1966).
14. J. Hubbard and W. Marshall, *Proc. Phys. Soc.* **86,** 561 (1965).
15. B. E. F. Fender, A. J. Jacobson, and F. A. Wedgwood, *J. Chem. Phys.* **48,** 990 (1968).
16. A. J. Jacobson and B. E. F. Fender, *J. Chem. Phys.* **52,** 4563 (1970).
17. A. F. Andresen, *Acta. Chem. Scand.* **22,** 827 (1968).
18. T. J. A. Popma, C. Haas and B. van Laar, *J. Phys. Chem. Solids* **32,** 581 (1971).
19. B. van Laar, *Phys. Rev.* **156,** 654 (1967).
20. T. Hamasaki, T. Hashimoto, Y. Yamaguchi, and H. Watanabe, *Solid State Commun.* **16,** 895 (1975).

21. J. A. Wilson, *Adv. Phys.* **21,** 143 (1972).
22. M. Cyrot, *Phil. Mag.* **25,** 1031 (1972).
23. J. Dijkstra, H. H. Weitering, C. F. van Bruggen, C. Haas, and R. A. de Groot, *J. Phys.: Condens. Matter* **1,** 9141 (1989).
24. J. Dijkstra, C. F. van Bruggen, C. Haas, and R. A. de Groot, *J. Phys.: Condens. Matter* **1,** 9163 (1989).
25. E. F. Bertaut, G. Roult, R. Aleonard, R. Pauthenet, M. Chevreton, and R. Jansen, *J. Phys.* (*Paris*) **25,** 582 (1964).
26. J. B. Goodenough, "Magnetism and the Chemical Bond," Chap. III. Wiley, New York, 1963.
27. R. Sachidanandam, T, Yildirim, A. B. Harris, A. Aharony, and O. Entin-Wohlman, *Phys. Rev. B* **56,** 260 (1997).
28. Th. Sinnemann, M. Mitag, M. Rosenberg, A. Ehmann, T. Fries, G. Mayer-von Kürthy, and S. Kemmler-Sack, *J. Mag. Magn. Mater.* **95,** 175 (1991).
29. J. M. Cadogan and S. A. Dann, *J. Mag. Magn. Mater.* **131,** L5 (1994).